Journal of Colloid and Interface Science 704 (2026) 139470

Contents lists available at ScienceDirect

Journal of Colloid And Interface Science

journal homepage: www.elsevier.com/locate/jcis

Controlled fabrication of highly ordered platinum nanostructures using pulsed electrodeposition

Joshua S. White [a], Samina Akbar [a], Adam Squires [b], Diego Alba-Venero [c], Nicholas J. Terrill [d], Iris Nandhakumar [a,*]

[a] Department of Chemistry, University of Southampton, Southampton, SO17 1BJ, UK
[b] Department of Chemistry, University of Bath, South Building, Soldier Down Ln, Claverton Down, Bath, UK
[c] ISIS Neutron and Muon Source, Rutherford Appleton Laboratory, Didcot OX11 0QX, UK
[d] Diamond Light Source, Diamond House, Harwell Science and Innovation Campus, Didcot, Oxfordshire OX11 0DE, UK

GRAPHICAL ABSTRACT

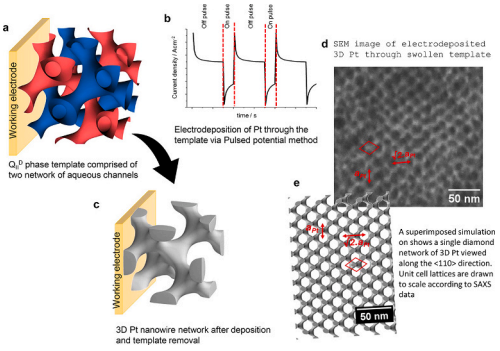

ARTICLE INFO

Keywords:
Pulse electrodeposition
Soft-templating
Single diamond phase
Platinum
3D nanowire network

ABSTRACT

Pulsed potential (PP) electrodeposition was utilized for the first time to fabricate three-dimensional (3D) platinum (Pt) nanostructures within phytantriol-based double diamond cubic templates, both with or without 20 % *w*/w Brij-56 as a pore swelling agent. Unlike conventional direct potential (DP) deposition, the PP approach yielded Pt nanostructures with markedly enhanced uniformity and superior lattice ordering. Small Angle X-ray Scattering (SAXS) revealed that PP-grown structures exhibited sharp, well-defined Bragg peaks corresponding to lattice parameters of 134.2 ± 2.1 Å without Brij-56 and 236.7 ± 2.5 Å with 20 % *w*/w Brij-56, whereas DP-grown structures showed broader, less distinct peaks with smaller lattice parameter (130.7 ± 1.9 Å and 197.1 ± 2.8 Å, respectively). Notably, In-situ SAXS measurements provided real-time insights into the evolution of 3D Pt nanostructures, enabling direct monitoring of orientational and lateral ordering within the templated phases. High resolution SEM further confirmed the superior quality of PP-grown structures, revealing highly ordered 3D nanowire network with uniform pore sizes of 89.5 ± 1.3 (without Brij-56) and 102.0 ± 0.7 Å (with 20 % *w*/w Brij-56). Overall, these findings highlight the effectiveness of PP electrodeposition in mitigating structural inhomogeneities, establishing it as a powerful strategy for fabricating well-ordered 3D Pt nanostructures.

* Corresponding author.
E-mail address: iris@soton.ac.uk (I. Nandhakumar).

https://doi.org/10.1016/j.jcis.2025.139470
Received 9 September 2025; Received in revised form 19 October 2025; Accepted 11 November 2025
Available online 12 November 2025

1. Introduction

Lyotropic liquid crystalline phases of lipid amphiphiles can act as structure-directing agents to guide the formation of well-ordered nanostructured inorganic or metallic materials. Once the desired material has been deposited either chemically or electrochemically within the lipid template, the lipid can be removed, leaving behind a nanostructured material that retains the ordered framework of the original lipid template [1–3]. This approach offers a versatile method for fabricating nanostructures with distinct geometries whose pore size can be precisely controlled, making them promising candidates for many potential applications in catalysis, sensing, energy storage, and nanotechnology [4–6]. Recently the use of bicontinuous lipid cubic phases of phytantriol has emerged as an attractive route for the fabrication of robust periodic nanoarchitectures that were found to be stable in different environments [3,7].

In the present work we report the first results of highly ordered 3D nanostructures of Pt with enhanced lattice ordering and uniformity that were electrochemically deposited via pulsed deposition from phytantriol-based bicontinuous lipidic cubic phases in the presence and absence of Brij-56. This is in contrast to earlier studies which employed direct electrodeposition to produce Pt nanostructures with single diamond morphology [3]. The addition of 0 to 20 % Brij-56 (*w*/w) in phytantriol was found to reduce the interfacial curvature of the lipid bilayer in the template under excess hydration conditions [2], leading to a swelling of its lattice parameter and to that of the deposited Pt material. It was further reported that the addition of more than 15 % (*w*/w) of Brij-56 to the phytantriol template mixture resulted in the broadening of the Small Angle X-ray Scattering (SAXS) peaks of the nano-templated Pt material. This peak broadening was attributed to the material's inhomogeneity. In addition the relationship between the Pt lattice parameter and that of the phytantriol template, a(Pt) = 2 x a(QII^D), was not maintained when using the swollen template [2]. A study conducted by Richardson et al. confirmed the inhomogeneity of Pt when grown by direct electrodeposition through a phytantriol/Brij-56 template [7].

Controlling atomic defects and achieving structural uniformity remains a significant challenge when DP deposition is employed. In contrast, PP deposition has emerged as a more effective approach for reducing roughness and improving the morphology of deposited materials, particularly in template assisted systems [8–14]. For instance, PP deposition has enabled the uniform filling of template pores, leading to the fabrication of highly ordered, ultra-long metal nanowires [13,15]. It has also facilitated the growth of stable, vertically aligned cylindrical single crystals of copper with high aspect ratios, as well as single crystalline antimony nanowires [14,16]. Furthermore, PP deposition provides precise control over the structure, composition, and crystallinity of the deposited material [10,13–15,17]. Key deposition parameters such as pulse time and deposition potential governs the nucleation rate, particle size, and morphology [18], while the resting time between pulses strongly influences the homogeneity of the resulting nanowires [15]. Pulsed potential deposition has also been applied previously to control the morphology of Pt nanostructures [19,20]; however, this study represents the first demonstration of its use to fabricate 3D Pt nanostructures within soft templates, establishing a key novelty of our work.

In the present study, we employed a cathodic pulse during PP to promote the creation of a high density of nucleation sites, while keeping the pulse duration short enough to prevent depletion of Pt cations near the electrode surface. The electrodeposition of Pt from hexachloroplatinic acid (HCPA) proceeds according to the following redox reaction:

$$PtCl_6^{2-} + 4e^- \rightarrow Pt(s) + 6Cl^-$$

Each cathodic pulse was followed by a resting pulse to allow replenishment of cations, and the cycle was repeated until the desired amount of material had been deposited. A schematic of this process that illustrates Pt growth within the aqueous channels of the phytantriol template using pulsed electrodeposition is shown in Fig. 1.

Although pulsed electrodeposition has been used to tailor the morphology of Pt films and nanowires, its application within lyotropic cubic phase templates of phytantriol to yield three-dimensional single-diamond Pt nanostructures has not been demonstrated previously. This work represents the first integration of pulsed electrochemical control with soft templating, enabling enhanced structural fidelity, orientation, and ordering compared to prior direct-potential deposition approaches.

The highly ordered, high-surface-area Pt nanostructures produced here are particularly attractive for electrocatalysis (e.g., oxygen reduction and hydrogen evolution), plasmonic sensing, and energy storage devices such as micro-supercapacitors. The improved structural uniformity achieved by pulsed deposition can enhance catalytic turnover and long-term stability compared with conventionally deposited Pt films.

2. Results and discussion

We will refer to samples of phytantriol, with and without 20 % Brij-56 (*w*/w) as swollen and unswollen templates respectively. The templates were prepared as thin films on gold (Au) DVD substrates which were placed inside an electrochemical cell that was filled with excess hexachloroplatinic acid (HCPA) solution for SAXS analysis on beamline I22 at Diamond Light Source. SAXS patterns shown in Fig. 2 reveal Bragg peaks in the ratio of $\sqrt{2}$, $\sqrt{3}$, $\sqrt{4}$, $\sqrt{6}$ which can be indexed to a *Pn3m* space group. This confirmed that both swollen and unswollen templates formed a double diamond cubic phase (Q_{II}^D). Important parameters extracted from the SAXS pattern are summarised in Table 1 which agrees well with existing literature values [2]. The water channel width is estimated by using the formula $d_w = 2(0.391a(Q_{II}^D)\text{-}l)$, which increased from 2.7 nm ± 0.2 with no addition of Brij-56 to 7.2 ± 0.3 nm when 20 % Brij-56 is present.

PP deposition of Pt within the template was carried out by applying a potential of +0.4 V vs SCE for 0.3 s, during which no deposition occurred (referred to as the 'off pulse'). This was followed by applying a potential of −0.245 V vs SCE for 0.1 s, at which Pt deposition took place (referred to as the 'on pulse'). For comparison, a number of Pt films were also produced by applying a constant potential of −0.245 V vs SCE using DP deposition. SAXS was performed on the resulting Pt films to analyse their structure. The 1D integrated SAXS patterns are shown in Fig. 3 and the results extracted from these are summarised in Table 2.

Fig. 3a reveals that Pt nanostructures grown by PP from a Q_{II}^D template (in the absence of Brij-56) exhibited three Bragg peaks with a peak ratio of $\sqrt{3}$, $\sqrt{8}$, and $\sqrt{11}$. These peaks can be indexed to a single diamond phase with a space group *Fd3m*. The unit cells are approximately twice as large as those of the original template, irrespective of the deposition method used. This structure forms as the Pt metal selectively fills one of the two aqueous channels present within the template, resulting in asymmetric deposition. This has previously been observed in the deposition of Pd [21], Bi_2S_3 [22], and Pt. [3]

The lattice parameter values of Pt nanostructures fabricated by DP and PP deposition from unswollen templates, are estimated to be 130.7 ± 1.9 Å and 134 ± 2.1 Å, respectively. In both cases, the lattice parameter can be calculated using $a(Pt) = 2 \times a\,(Q_{II}^D) = 138$ Å, consistent with previous report [3]. The estimated pore sizes for these unswollen templates were 68.5 ± 1.1 Å for DP and 69.7 ± 0.5 Å for PP deposition, indicating slightly larger and more uniform pores under pulsed deposition. For swollen templates, DP deposition yielded a lattice parameter of 197.1 ± 2.8 Å, which is 23 % smaller than the expected value of 254 Å ($a(Pt) = 2 \times a(Q_{II}^D) = 2 \times 127$ Å), indicative of significant structural deviations likely caused by the swelling agent. The corresponding pore size was 89.5 ± 1.3 Å, reflecting both lattice shrinkage and broader pore size distribution compared to the template. Although the precise cause is unclear, previous studies suggest that under excess hydrated, temperature increases can reduce the unit cell size of the Q_{II}^D phase [23].

Localized heating during electrodeposition, combined with the increased flexibility of phytantriol-Brij-56 mixtures, likely contributes to this shrinkage [1,7]. The presence of 20 % *w*/w Brij-56 is known to increase deposition current sixfold and enhance water channels diffusion sevenfold [2], potentially intensifying localized heating during DP deposition and leading to a reduction in the lattice parameter of the deposited Pt.

In contrast, PP deposition, in which the deposition potential is applied in short bursts followed by resting periods, governs the transient kinetics of nucleation and diffusion differently compared to DP deposition. This allows more controlled and uniform growth even in the presence of Brij-56. As a result, Pt nanostructures grown by PP deposition exhibited a lattice parameter of 236.7 ± 2.5 Å, much closer to the expected value of 254 Å, with an estimated pore size of 102 ± 0.7 Å. The narrow standard deviation in pore size under PP deposition demonstrates more uniform and well-defined channels compared to DP deposition, highlighting the method's ability to maintain structural fidelity even in swollen templates.

In the SAXS patterns shown in Fig. 3(a), 3D Pt nanostructures grown from unswollen templates via DP deposition revealed only two Bragg peaks ($\sqrt{3}$, $\sqrt{8}$), whereas Pt grown using PP deposition clearly revealed three distinct peaks ($\sqrt{3}$, $\sqrt{8}$, $\sqrt{11}$). Further, the SAXS peaks of the Pt nanostructures grown via DP deposition are broader compared to those grown by PP deposition. The FWHM values for the $\sqrt{3}$ reflection of the Pt nanostructures grown by PP and DP deposition respectively are presented in Table 3. The FWHM values are significantly smaller for the Pt nanostructures grown via PP deposition. This is more noticeable in Fig. 3 (b), where Pt nanostructures are grown from swollen templates.

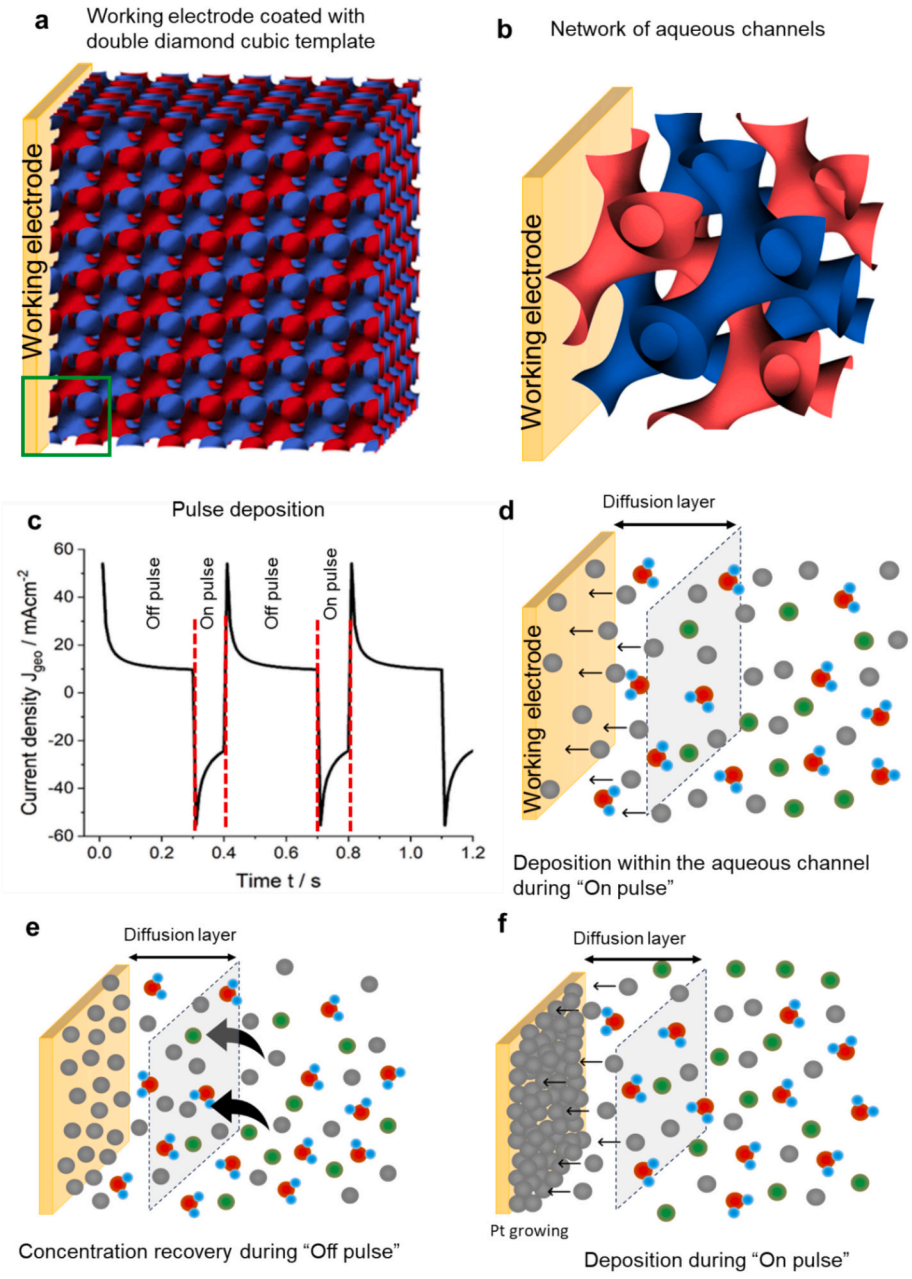

Fig. 1. a) Working electrode coated with thin film of cubic template, b) zoomed in image from boxed area of b showing 3D network of aqueous channels of double diamond cubic template, c) a current-time transient of first three cycles of Pt electrodeposited onto a Au-DVD electrode coated with phytantriol containing 20 % Brij-56 with a 0.1 s on pulse of −0.245 V vs SCE and an off pulse of 0.3 s at 0.4 V vs SCE from an 8 wt% HCPA solution, d) deposition of Pt during on pulse, e) concentration recovery during off pulse, f) Pt growth in subsequent on pulse.

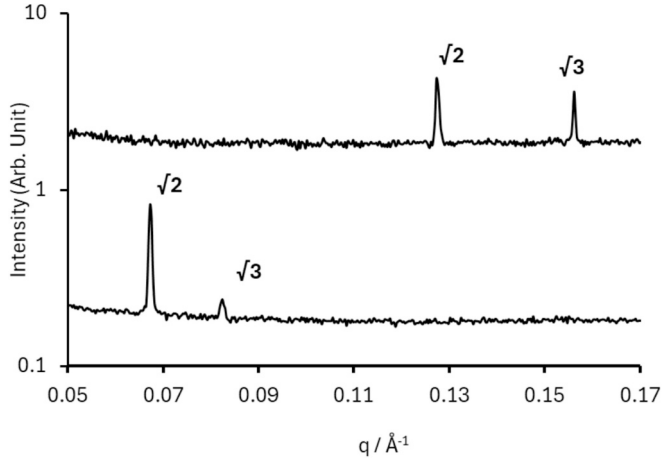

Fig. 2. 1D integrated SAXS patterns of phytantriol with differing amounts of Brij-56 in excess HCPA solution recorded at room temperature.

Table 1
A table reporting the key results from SAXS of phytantriol and Brij-56 mixtures in excess HCPA conditions.

Template	Phase	Lattice parameter a (Å^{-1})	Water channel width (nm)
Unswollen	Q_{II}^{D}	69.2 ± 0.2	2.7 ± 0.2
Swollen	Q_{II}^{D}	127.0 ± 0.3	7.2 ± 0.3

Peak broadening may result from finite domain size effects, as described by the Scherrer equation [24], or from lattice parameter variations within the sample, leading to a distribution of lattice spacings [1]. These causes can be distinguished by analyzing peak widths: domain size effects produce consistent broadening across all peaks, while lattice variations cause greater broadening at higher scattering angles, with width increasing with peak position. Akbar et al. [2] first identified peak broadening in SAXS patterns for Pt nanostructures grown through swollen templates via DP deposition, attributing this effect to variations in the lattice parameter throughout the sample. They observed that the widths of the $\sqrt{3}$ and $\sqrt{8}$ reflections were inconsistent and increased approximately by 1/d, strongly suggesting that inhomogeneity within the sample was the cause. We have achieved much greater uniformity in lattice parameters for the Pt nanostructures when grown by PP deposition, as evidenced by the sharper, more distinct SAXS peaks, the appearance of higher order Bragg reflections, and narrower FWHM values. This is also evidenced by the pore size distribution. Variation in the pore size is much more prominent in the DP grown structures whereas PP grown structures show less variation in pore size distribution.

To simultaneously monitor the growth of Pt within the template during the deposition process, in-situ SAXS measurements were carried out on beamline I22 at Diamond Light Source using a custom-made 3D printed electrochemical cell. Fig. 4 shows 1D integrated SAXS images of Pt electrodeposited from swollen and unswollen templates when a steady potential of −0.245 V vs SCE was applied (DP mode) and when pulses were applied (PP mode) at different times. Initially, before any potential is applied, both Pt nanostructures revealed only the lipid signals, with $\sqrt{2}$, $\sqrt{3}$, $\sqrt{4}$, and $\sqrt{6}$ Bragg peaks corresponding to the double diamond phase of space group Pn3m. In case of the unswollen templates (cf. Fig. 4a), the lattice parameter of the Q_{II}^{D} template is estimated to be 69.2 ± 0.2 Å, whilst for the swollen templates (Fig. 4b), it is larger at 127.0 ± 0.3 Å. After applying on-pulses at −0.245 V for 0.1 s and off-pulses at 0.4 V vs SCE for 0.3 s for more than 700 cycles, a new peak appears in both cases, indicating the growth of Pt within the template. For unswollen templates, a peak emerges at q = 0.087 Å^{-1}, corresponding to the $\sqrt{3}$ reflection of the single diamond structure (Fd3m space group), with an estimated lattice parameter of 134.2 ± 2.1 Å. In contrast, for swollen templates, the new peak appears at q = 0.048 Å^{-1}, which may also be attributed to the $\sqrt{3}$ reflection of the single diamond structure, however exhibiting a larger lattice parameter of 236.7 ± 2.5 Å.

As the deposition progresses, higher order Bragg peaks appear indicating the clear formation of a single diamond structure in both cases. For unswollen templates, with deposition cycles exceeding 1000, the $\sqrt{8}$ and $\sqrt{11}$ Bragg peaks become distinguishable at q = 0.135 Å^{-1} and q = 0.164 Å^{-1}, respectively. For swollen templates, after more than 1400 deposition cycles, the $\sqrt{11}$ Bragg peak becomes evident at q = 0.076 Å^{-1}. In both cases, the intensity of the double diamond phase peaks diminishes whilst the peaks for the single diamond structure are amplified, confirming the formation of a Fd3m symmetry, where the Pt grows as a single diamond structure rather than through the lateral shift of two networks in a double diamond configuration after template removal [25]. This study also represents the first report in which higher order Bragg peaks in the SAXS profiles for single diamond Pt grown from phytantriol Q_{II}^{D} templates were observed. Previously, the structure symmetry was assumed to be based on the first peak for each phase, as no additional reflections were observed that could have further helped to identify the phase [2].

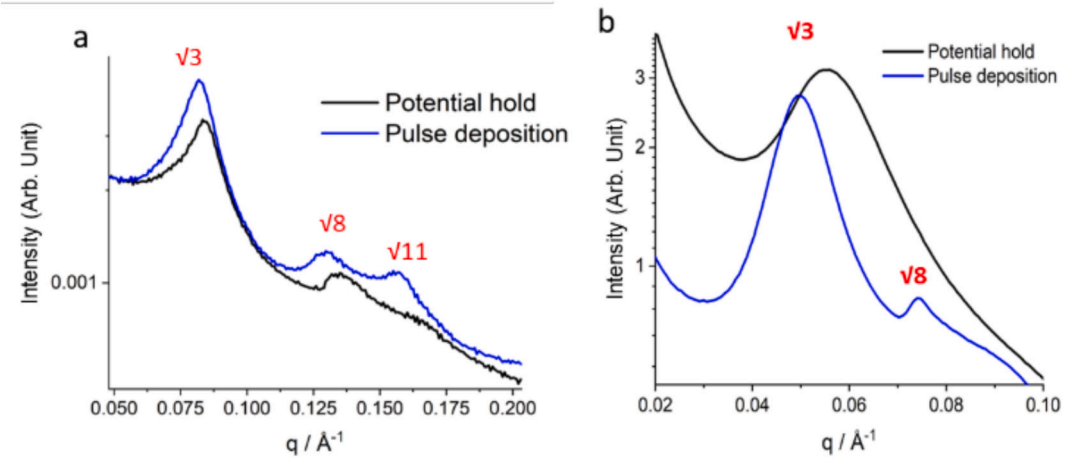

Fig. 3. 1D integrated SAXS patterns of Pt electrodeposited through (a) unswollen and (b) swollen phytantriol/Brij-56 templates using direct potential (DP) and pulsed potential (PP) regimes. Reflections are indexed to the single-diamond (Fd3m) structure, with peak ratios of $\sqrt{3}$, $\sqrt{8}$, and $\sqrt{11}$. The sharper, higher-order peaks observed for PP deposition indicate improved long-range order and structural uniformity compared to DP.

For comparison, Pt structures were also grown via DP deposition using swollen and unswollen templates. SAXS images recorded over time revealed the progression of Pt growth in unswollen (Fig. 4c) and swollen (Fig. 4d) templates. For the unswollen templates, only the first Bragg peak $\sqrt{3}$ is visible at deposition times greater than 2 min, and this peak is significantly broader, reflecting an increase in FWHM value. The higher order scattering peak $\sqrt{8}$ is weak, and difficult to distinguish, suggesting a poorly ordered nanostructure with a lack of long-range order. In the case of swollen templates, only a single broad first-order Bragg peak $\sqrt{3}$ is detected. Absence of higher order peaks further highlight the limitations of using DP deposition in achieving well-ordered structures.

2D SAXS imaging can be used to investigate the lateral ordering and orientation of Pt structures grown within the template. Previous studies using out-of-plane GISAXS demonstrated that Pt electrodeposited inside a swollen template was oriented for templates containing up to 15 wt% Brij-56. However if Brij-56 concentrations exceeded 15 wt%, this orientation disappeared, and only a polydomain ring was observed [25]. 2D SAXS images taken in and out of plane of Pt electrodeposited through phytantriol containing 20 % Brij-56 are shown in Fig. 5. Fig. 5(a) reveals that Pt grown by DP electrodeposition through a swollen template of phytantriol with 20 % Brij-56 exhibited only a polydomain ring in out-off-plane GISAXS, with no observed orientation. In contrast, Fig. 5(b) shows that Pt produced via PP electrodeposition also displayed distinct spots which indicates an oriented single diamond phase.

We believe that the improvement in the orientation and lateral ordering of Pt nanostructure electrodeposited in pulsed mode can be attributed to the “off” pulse period, which allows the system time to relax.

FEG-SEM images of Pt electrodeposited via pulse mode from the swollen template are shown in Fig. 6. The simulated projections in Fig. 6d reveal the Pt nanowire networks which are aligned along the (110) direction when viewed from the top, with unit cell dimensions drawn to scale based on SAXS data, matching the lattice parameter values estimated from SEM.

SEM, for the first time, is used to image the single diamond phase of Pt, permitting visualisation of the nanostructures without the need for destructive sample preparation as necessitated by TEM. The SEM images clearly reveal the presence of nanometer sized pores and the 3D array of interconnected nanowires for Pt that was deposited by PP through swollen templates. Further, the visibility of pores in TEM is highly dependent on their orientation which can make it more difficult to observe the presence of pores, especially when samples are not perfectly aligned. SEM images, recorded for pulse-deposited films, showed enhanced visibility of the pores due to their alignment in the plane of the beam, as shown in Fig. 6. The enhanced structural regularity and improved interconnectivity of the PP-grown Pt nanostructures are anticipated to provide superior mechanical and electrochemical stability by minimizing localized current hotspots and stress points. This expectation is consistent with the smaller variations in lattice parameter and pore size observed from SAXS analysis, which indicate a more mechanically robust nanostructure.

3. Experimental

All chemicals were used as received without further purification. Phytantriol was purchased from TCI Europe (98 % purity). Hexachloroplatinic acid (HCPA) (8 wt% in water) was purchased from Aldrich. All solutions were prepared using ultrapure Milli-Q water. Brij-56 was purchased from Fluka Chemicals.

Table 3
The FWHM values calculated for $\sqrt{3}$ reflection of the cubic templates and Pt nanostructures grown via pulse deposition and potential hold methods.

Template	FWHM Template $\sqrt{3}$ reflection	FWHM Pt $\sqrt{3}$ reflection Potential hold	FWHM Pt $\sqrt{3}$ reflection Pulse mode
0 % Brij	6.78×10^{-4}	0.015	0.013
20 %Brij	2.33×10^{-3}	0.018	0.012

3.1. Electrode preparation

Au-DVD from Delkin Devices were used as a working electrode by cutting them to size and removing the insulating polymer layer to expose the gold surface. The surface was masked using nail varnish with a 1×1 cm^2 area exposed to the electrolyte solution.

To prepare the electrodes for electrodeposition, the Au DVD electrodes were dip coated in a phytantriol: ethanol or phytantriol/Brij-56: ethanol mixture in a ratio of 1:2 by weight and allowed to dry for not less than an hour under ambient conditions so that the ethanol evaporated, leaving behind a thin film of phytantriol or phytantriol/Brij-56 on the surface of electrode. Thin film coated electrodes were soaked in HCPA solution prior to electrodeposition for at least 10 min to allow the lipid film to hydrate forming double diamond cubic templates.

3.2. Electrodeposition

HCPA (8 wt% in water) was used as a platinum precursor for the electrodeposition of templated Pt. Electrodeposition experiments were performed using a three-electrode setup consisting of working electrode, Saturated Calomel reference electrode (SCE), and a platinum gauze counter electrode using an Ivium VERTEX potentiostat controlled using IviumSoft. For direct potential electrodeposition, potential was stepped from +0.4 to −0.245 V vs SCE for a set period of time until a desired amount of charge was passed. Pulse potential deposition was carried out by applying a potential of +0.4 V vs SCE for 0.3 s, during which no deposition occurs, naming as the ‘off pulse’, followed by applying a potential of −0.245 V vs SCE for 0.1 s, at which Pt deposition takes place, named as ‘on pulse’. Each PP deposition experiment consisted of approximately 700–1400 pulse cycles, depending on template swelling and desired film thickness. The cathodic pulse of −0.245 V vs SCE (0.1 s) was chosen to promote nucleation without mass-transport depletion, while the anodic off-pulse at +0.4 V vs SCE (0.3 s) permitted ionic relaxation and replenishment. These parameters were optimized empirically to maximize lattice ordering observed in SAXS.

3.3. Removal of the template

After Pt electrodeposition, the working electrodes were soaked in ethanol for at least 30 min, followed by rinsing with water. This procedure was repeated twice to ensure complete removal of the lipid template, and the electrodes were then left to dry under ambient conditions.

Table 2
Summary of key results based on SAXS of Pt nanostructures deposited from phytantriol and Brij-56 mixtures using potential hold and pulse deposition.

Template	Phase	a (Q_{II}^{D} template) (Å)	a (Pt) (potential hold) (Å)	Estimated pore size (potential hold) (Å)	a (Pt) (pulse deposition) (Å)	Estimated pore size (pulse deposition) (Å)
Unswollen	Single diamond	69.2 ± 0.2	130.7 ± 1.9	68.5 ± 1.1	134.2 ± 2.1	69.7 ± 0.5
Swollen	Single diamond	127.0 ± 0.3	197.1 ± 2.8	89.5 ± 1.3	236.7 ± 2.5	102.0 ± 0.7

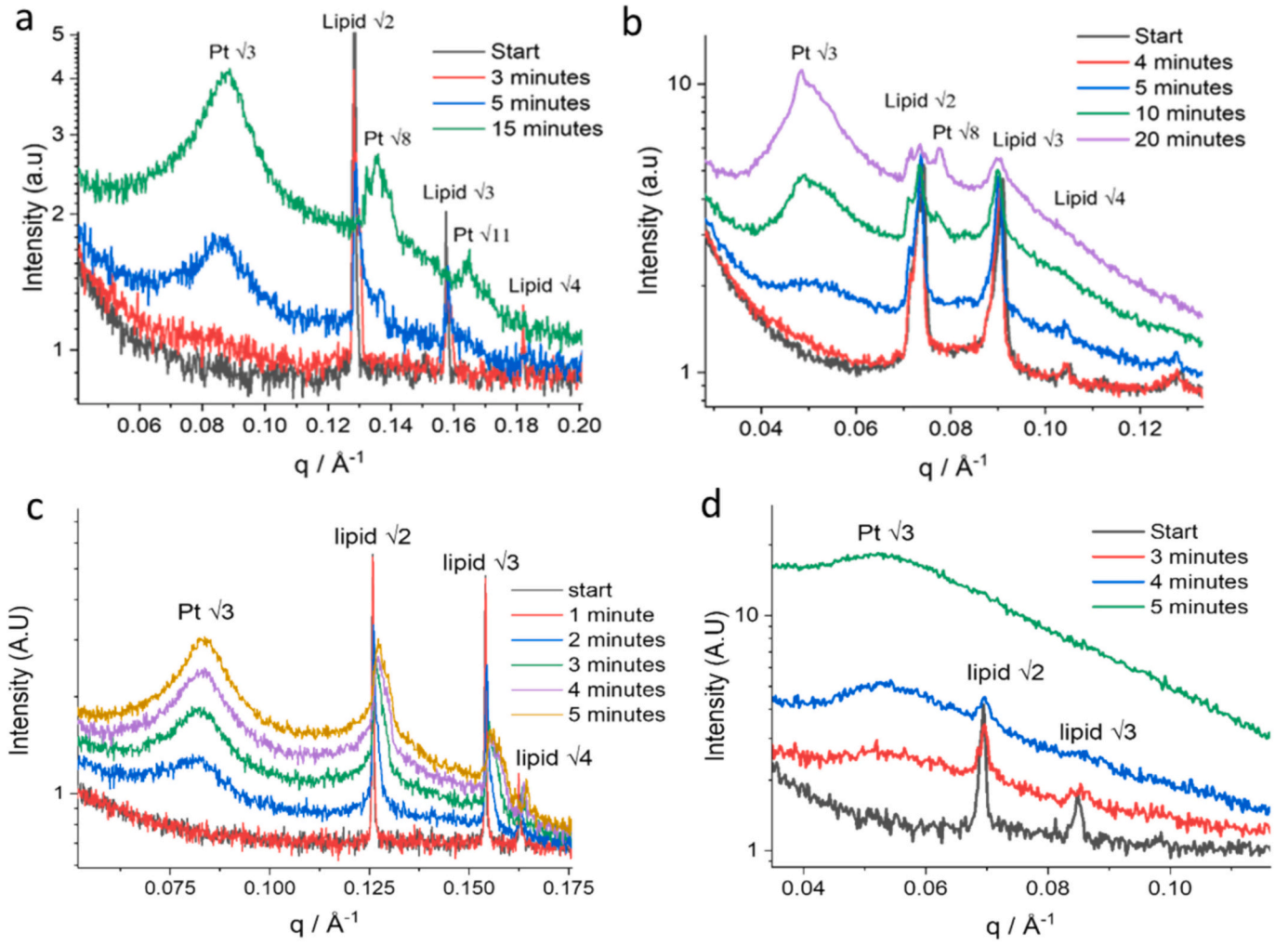

Fig. 4. 1D integrated SAXS patterns recorded at different time intervals during the electrodeposition of platinum via PP (a, b) and DP (c, d) from a solution of 8 wt% HCPA solution while utilizing unswollen (a, c) and swollen (b, d) templates. In case of DP, potential was held at −0.245 V vs SCE for specific period of time. For PP deposition, an on pulse of 0.1 s at −0.245 V vs SCE and an off pulse at 0.4 V vs SCE for 0.3 s were applied for a number of cycles.

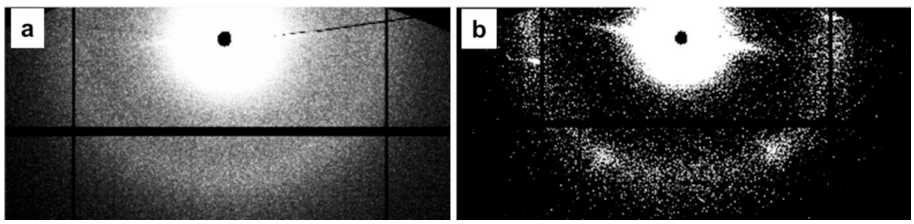

Fig. 5. 2D SAXS images taken in an out of plane orientation of Pt electrodeposited through phytantriol/Brij-56(20 wt%) on Au foil electrodes via DP (a) and PP (b) electrodeposition, along with blue circles which are an overlay of the predicted spot pattern locations for the single diamond phase orientated with the (111) plane parallel to the electrode surface. (For interpretation of the references to colour in this figure legend, the reader is referred to the web version of this article.)

3.4. Small angle X-ray scattering (SAXS)

SAXS experiments were performed on beamline 122 at the Diamond light source. A camera length of 4.5 m was used with a beam energy of 12.4 keV. For the in-situ experiments conducted on the offline SAXS instrument, Xeuss, at the Diamond Light Source, a camera length of 1.5 m was used. The experiments utilized a beam energy of 9.2 keV, generated by a Ga MetalJet source.

In-situ SAXS during electrodeposition was performed using a custom-made 3D printed electrochemical cell. The in-situ measurements, shown in Fig. 5, were performed in transmission mode with the X-ray beam going through the windows of the cell and the phytantriol or phytantriol/Brij-56 modified Au-DVD electrodes perpendicular to the incoming beam.

3.5. SEM imaging

SEM imaging was performed on a Carl Zeiss Sigma 500 VP FE-SEM equipped with Inlens Duo SE and BSE switchable detectors (1.3 nm at 1 kV 0.8 nm at 15 kV).

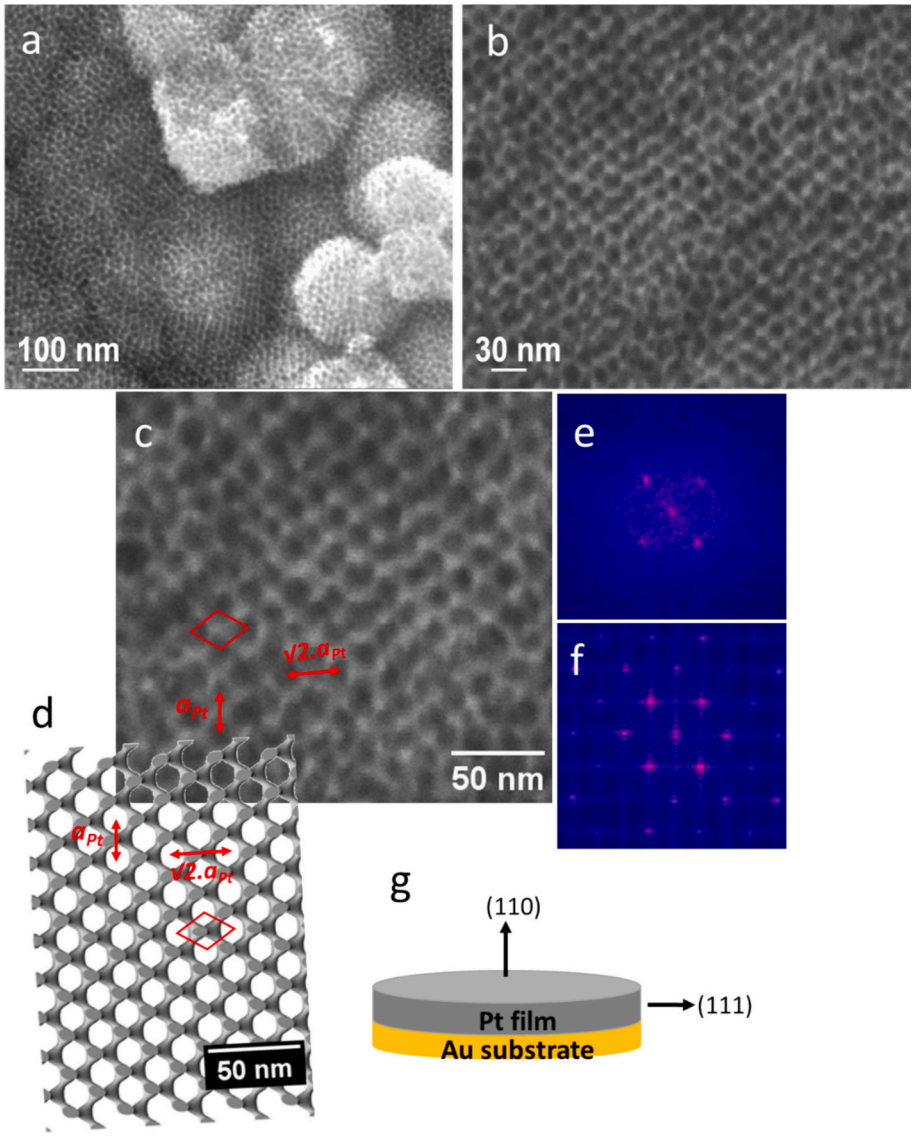

Fig. 6. SEM images (a-c) taken at different magnifications of Pt electrodeposited through swollen template via PP electrodeposition from a solution of 8 wt% HCPA solution. A superimposed simulation on "d" shows a single diamond network of Pt viewed along the ⟨110⟩ direction. Unit cell lattices are drawn to scale according to SAXS data, (e) FFT generated from c, and (f) FFT generated from d, g) Orientation of Pt structure.

4. Conclusions

In conclusion, this study has clearly demonstrated that pulsed potential (PP) electrodeposition significantly enhances the structural quality and uniformity of 3D platinum nanostructures when compared to direct potential (DP) electrodeposition. The SAXS analysis revealed that PP electrodeposition from phytantriol-based templates, both swollen and unswollen, yielded platinum nanostructures with substantially improved lattice ordering, characterized by sharper and more distinct Bragg peaks. These results highlight the ability of PP electrodeposition to mitigate structural inhomogeneities commonly encountered in DP deposition processes. Furthermore, in-situ SAXS investigations provided valuable insights into the real-time formation and ordering process of Pt nanostructures, highlighting the advantages of transient deposition kinetics inherent in PP methods. High-resolution SEM imaging complemented these findings, visually confirming the enhanced structural order and uniform pore dimensions achieved through PP electrodeposition. The superior uniformity, lattice precision, and structural integrity of the Pt nanostructures fabricated via PP methods have significant implications for their practical applications. Such highly ordered and uniform nanostructures are expected to exhibit improved performance in catalytic reactions, sensing applications, and energy storage devices, where structural consistency directly impacts functional efficiency.

Overall, the advancement in template-assisted electrodeposition techniques presented herein establishes PP electrodeposition as a robust method for fabricating precise and well-defined nanoscale architectures. This methodology opens new avenues for the controlled fabrication of metallic nanostructures, potentially advancing numerous technological fields reliant on nanoscale precision and uniformity.

Future work will focus on electrochemical characterization of the pulsed-deposited Pt nanostructures, including cyclic voltammetry and impedance spectroscopy, to quantitatively assess charge-transfer kinetics and long-term stability. Such measurements will enable a direct correlation between the structural improvements demonstrated here and the electrochemical performance of the electrodes.

Authors contribution

All of the authors contributed to the writing of the manuscript. All

authors have given their approval to the final version of the manuscript.

CRediT authorship contribution statement

Joshua S. White: Investigation, Data curation. **Samina Akbar:** Writing – original draft. **Adam Squires:** Writing – review & editing. **Diego Alba-Venero:** Writing – review & editing, Supervision. **Nicholas J. Terrill:** Supervision, Funding acquisition. **Iris Nandhakumar:** Writing – original draft, Supervision, Project administration, Funding acquisition.

Declaration of competing interest

The authors declare the following financial interests/personal relationships which may be considered as potential competing interests: Iris Nandhakumar reports financial support was provided by Engineering and Physical Sciences Research Council. If there are other authors, they declare that they have no known competing financial interests or personal relationships that could have appeared to influence the work reported in this paper.

Acknowledgements

I.N. acknowledges financial support by the Engineering and Physical Sciences Research Council (EPSRC) for Grant No. EP/X012840/1. The authors would like to thank Diamond Light Source for beamtime (NT33748, NT35376, NT35348) and the staff of beamline I22 for assistance with data collection. J.W. would like to acknowledge Diamond Light Source and ISIS for co-sponsoring a PhD studentship.

Appendix A. Supplementary data

Supplementary data to this article can be found online at https://doi.org/10.1016/j.jcis.2025.139470.

Data availability

Data for this article are available from https://doi.org/10.5258/SOTON/D3508.

References

[1] G.S. Attard, P.N. Bartlett, N.R. Coleman, J.M. Elliott, J.R. Owen, J.H. Wang, Science 278 (1997) 838–840.
[2] S. Akbar, J. Boswell, S. Waters, S. Williams, J.M. Elliott, A.M. Squires, ACS Appl. Nano Mater. 4 (2021) 5717–5725.
[3] S. Akbar, J.M. Elliott, M. Rittman, A.M. Squires, Adv. Mater. 8 (2013) 1160–1164.
[4] J. Wordsworth, T.M. Benedetti, S.V. Somerville, W. Schuhmann, R.D. Tilley, J. J. Gooding, Angew. Chem. Int. Ed. 61 (2022) e202200755.
[5] J.S. White, W. Liu, S.C. Perry, S. Akbar, D. Alba-Venero, N.J. Terrill, A. Squires, I. Nandhakumar, ACS Omega 10 (2025) 8082–8088.
[6] X. Zhang, Y. Xu, C. Valenzuela, X. Zhang, L. Wang, W. Feng, Q. Li, Light Sci Appl 11 (2022) 223.
[7] S. Richardson, M. Burton, P. Staniec, I. Nandhakumar, N. Terrill, J. Elliott, A. Squires, Nanoscale 8 (2016) 2850–2856.
[8] A. Belov, S. Gavrilov, V. Shevyakov, E. Redichev, Appl. Phys. A 102 (2011) 219–223.
[9] F. Cheng, H. Wang, Z. Sun, M. Ning, Z. Cai, M. Zhang, Electrochem. Commun. 10 (2008) 798–801.
[10] A. Esmaeili, M.A. Kashi, A. Ramazani, A. Montazer, J. Magn. Magn. Mater. 397 (2016) 64–72.
[11] E. Premalal, R. Rajapakse, A. Konno, Electrochim. Acta 56 (2011) 9180–9185.
[12] K.-R. Yeo, J. Eo, M.J. Kim, S.-K. Kim, J. Electrochem. Soc. 169 (2022) 112502.
[13] G. Sauer, G. Brehm, S. Schneider, K. Nielsch, R. Wehrspohn, J. Choi, H. Hofmeister, U. Gösele, J. Appl. Phys. 91 (2002) 3243–3247.
[14] Y. Zhang, G. Li, Y. Wu, B. Zhang, W. Song, L. Zhang, Adv. Mater. 14 (2002) 1227–1230.
[15] J. Azevedo, C. Sousa, J. Ventura, A. Apolinario, A. Mendes, J. Araujo, Mater Res Express 1 (2014) 015028.
[16] D. Dobrev, J. Vetter, N. Angert, R. Neumann, Appl. Phys. A 69 (1999) 233–237.
[17] M. Almasi Kashi, A. Ramazani, N. Akhshi, E. Khamse, Z. Fallah, J. Nanostruct. 1 (2011) 249–255.
[18] F. Ye, J. Li, T. Wang, Y. Liu, H. Wei, J. Li, X. Wang, J. Phys. Chem. C 112 (2008) 12894–12898.
[19] J. Liu, X. Wang, Z. Lin, Y. Cao, Z. Zheng, Z. Zeng, Z. Hu, Electrochim. Acta 136 (2014) 66–74.
[20] C. Stegmann, F. Muench, M. Rauber, M. Hottes, J. Brötz, U. Kunz, S. Lauterbach, H.-J. Kleebe, W. Ensinger, RSC Adv. 4 (2014) 4804–4810.
[21] M. Burton, A. Selvam, J. Lawrie-Ashton, A. Squires, N. Terrill, I. Nandhakumar, ACS Appl. Mater. Interfaces 10 (2018) 37087–37094.
[22] M.R. Burton, C. Lei, P.A. Staniec, N.J. Terrill, A.M. Squires, N.M. White, I. S. Nandhakumar, Sci. Rep. 7 (2017) 6405.
[23] J. Barauskas, T. Landh, Langmuir 19 (2003) 9562–9565.
[24] P. Scherrer, Colloid Chem. A Textbook (1912) 387–409.
[25] S. Richardson, M. Burton, X. Luo, P.A. Staniec, I. Nandhakumar, N.J. Terrill, J. M. Elliott, A. Squires, Nanoscale 9 (2017) 10227–10232.